sciendo

LATVIAN JOURNAL OF PHYSICS
AND TECHNICAL SCIENCES
2025, N 3

DOI: 10.2478/lpts-2025-0024

INVESTIGATING THE FEASIBILITY OF INTEGRATING VEGETATION INTO SOLAR CHIMNEY POWER PLANTS IN THE TAMANRASSET REGION

S. Ali[1,2] *, B. Djaouida[1]

[1] Faculty of Science and Technology,
University of Tamanrasset,
Tamanrasset, ALGERIA
[2] Materials and Energy Research Laboratory,
University of Tamanrasset,
Tamanrasset, ALGERIA
*e-mail: sellami2003@hotmail.com

The Solar Chimney Power Plant (SCPP) utilises a two-step procedure to transform solar energy into electricity. First, it uses a solar collector to turn sunlight into thermal energy. Then, this thermal energy is transformed into kinetic energy as it raises a chimney and finally into electrical energy via a wind turbine and generator. A numerical simulation of a prototype in Manzanares, Spain, was conducted using a 2D axi-symmetric model and computational fluid dynamics with an RNG k-turbulence model. The simulation also involved solving the radiative transfer equation with a two-band discrete ordinate radiation model. This study aims to evaluate the effect of vegetation beneath the collector roof on a solar chimney power plant's performance. Our research compared various designs of these power plants, both with and without vegetation. Three configurations were examined in this study: a standard power plant, a power plant with a secondary collector roof, and a power plant with both secondary and tertiary collector roofs. According to our findings, the system with secondary and tertiary collector roofs demonstrated the highest electricity generation capacity, yielding an annual output ranging from 34 to 80 kW. The findings indicate that adding vegetation into a solar chimney power plant is feasible but will most likely reduce the plant's energy generation.

Keywords: *Electrical generator, numerical simulation, solar chimney, solar energy, vegetation.*

1. INTRODUCTION

The growing need for energy and dependence on non-renewable fossil fuels has caused environmental concerns. Solar chimney power plants offer a promising solution as a clean energy source. The described system is a renewable energy technology that harnesses solar radiation to increase the internal energy of air, afterwards converting it into electrical energy through the utilisation of wind turbines. The concept of utilising air energy as a means of power generation was initially introduced by Spanish Colonel Cabanyes during the early 1900s [1]. In the 1980s, researchers put Cabanyes' idea to the test by building a prototype of a Solar Upwind Power Plant, also known as a Solar Chimney Energy System or Solar Tower [2]. Solar Upwind Power Plants are a clean and eco-friendly method of capturing solar energy to generate electricity [3]. The Solar Chimney Power Plant system represents a form of renewable energy generation that effectively converts solar energy into thermal energy, followed by the conversion of thermal energy into kinetic energy, and ultimately into electrical energy [4]. The Solar Chimney Power Plant was initially introduced by Professor Jörg Schlaich during the latter part of the 1970s. Subsequently, a prototype of this design was subjected to testing in Manzanares, Spain, during the early 1980s [5].

In recent times, several studies have undertaken an analysis of Solar Collector Performance Parameters (SCPP) utilising widely employed commercial Computational Fluid Dynamics (CFD) software packages, including FLUENT and TRNSYS [6]–[12]. A study by Ming et al. [13] analysed the impact of cross-wind velocity on SCPP performance. Cao et al. [10] evaluated SCPP performance through a design and simulation analysis using TRNSYS. In their 2007 simulation, Huang et al. [14] employed a Spanish prototype plant and utilised the Boussinesq model and DO to simulate natural convection and radiation, respectively. It was discovered that augmented solar radiation resulted in elevated temperature disparities and differential pressure at the intake and outflow of the collector, as well as at the transition section between the collection and the chimney.

In their study, Gholamalizadeh and Kim (2016) employed a three-dimensional computational fluid dynamics (CFD) analysis together with a two-band radiation model to replicate the greenhouse effect and heat transport within the system [9]. Their research underscores the importance of greenhouse effect simulations in assessing the performance of solar combined power and cooling (SCPP) systems. The study conducted by Guo et al. [15] involved the integration of radiation, solar load, and an actual turbine in a simulation to investigate various power-regulating strategies for solar chimney turbines. The researchers compared the outcomes obtained from a fan model with those obtained from an actual turbine.

The study conducted by Nasirivatan et al. (2015) examined the influence of Corona wind on the performance of solar chimneys [16]. In 2016, Ghalamchi et al. conducted an optimisation study on a pilot solar chimney configuration, consisting of a 3-meter height and a 3-meter collector [17]. Liu and Li (2020, 2021) conducted an assessment on the thermal efficiency of a solar chimney system incorporates a phase change material (PCM) [18], [19].

The study conducted by Attig et al. (2015) involved the comparison of a three-dimensional computational fluid dynamics (CFD) model of a solar chimney power plant (SCPP) with the Manzanares plant prototype [20]. The objective of the study was to investigate the operational aspects of SCPP in Tunisia. In their study, Akhtar and Rao conducted an analysis on the economic efficiency of a 200 MW supercritical coal-fired power plant (SCPP) located in Rajasthan, India [21].

The objective of this study is to investigate the feasibility of the incorporation of vegetation under the collector roof of a solar chimney.

2. PHYSICAL MODEL

A physical model of SCPP is established to examine the influence of buoyancy on flow and heat transfer. The design is based on the Manzanares power plant with a 194.6-meter-tall chimney (Hch) and 10.16-meter-wide diameter (rch). The collector has a radius (Rcol) of 122 meters and an average height (Hcol) of 1.85 meters, and the turbine is positioned 9 meters above the ground. The collector height increases to a maximum of 6 meters near the chimney base, which results in the airflow being directed upwards before reaching the turbine. The ground, serving as the energy storage medium, is assumed to be five meters thick. This design is illustrated in Fig. 1.

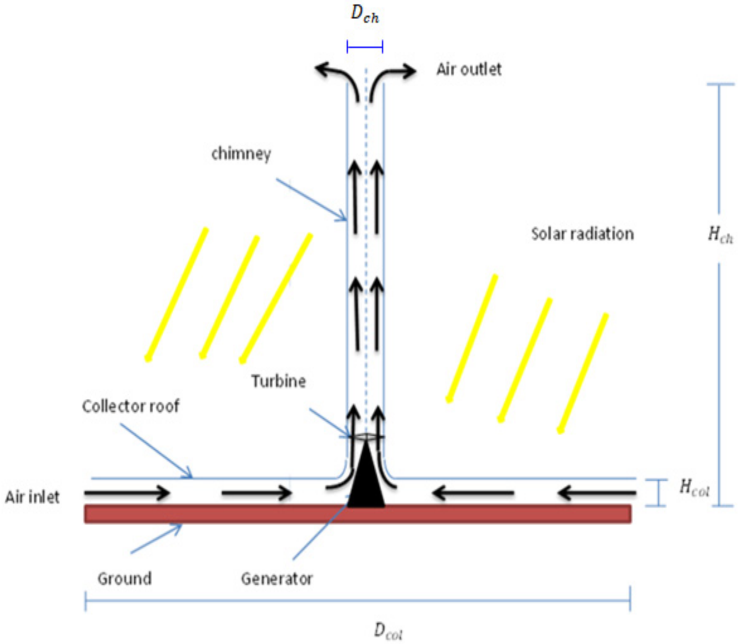

Fig. 1. A diagram of the solar chimney power plant system.

3. ELECTRICITY PRODUCTION

3.1. The Collector

The formula for the heat gained by air in the collector is as follows:

$$Q = \eta_{col.} A_{col.} G \, , \tag{1}$$

where $A_{col.}, G$ *and* η_{col} are the solar collector area ($A_{coll} = \pi R_{col}^{2}$), the solar radiation and the solar collector efficiency, respectively. Q represents also the generated heat due to the effect of the greenhouse in the collector and can be expressed as follows:

$$Q = C_{p.} m . \Delta T \, , \tag{2}$$

where $m = \rho_{air.} V_{ch} A_{ch}$. (3)

Then, the efficiency of the solar collector is described as follows:

$$\eta_{col.} = \frac{\rho_{air} V_{ch} A_{ch} C_{p} \Delta T}{A_{col} G} \, . \tag{4}$$

In this context, m represents the mass flow, A_{ch} denotes the surface area, and V_{ch} signifies the velocity at the entrance to the chimney.

3.2. The Chimney

As stated in [24], the chimney's efficiency is defined as follows:

$$\eta_{ch} = \frac{g . H_{ch}}{C_p T_a}, \tag{5}$$

where H_{ch} represents the height of the chimney, T_a stands for the ambient air temperature, and the flow power P_{tot} is expressed as follows:

$$P_{tot} = \eta_{ch} \, Q = \frac{g H_{ch}}{T_a} \rho_{col} V_{ch} \Delta T A_{ch} \, . \tag{6}$$

The pressure difference, ΔP_{tot}, created between the base of the chimney and its surroundings, is determined by:

$$\Delta P_{tot} = \rho_{col} g H_{ch} \frac{\Delta T}{T_a} . \tag{7}$$

3.3. The Turbine

Turbines are installed at the bottom of chimneys to transform the kinetic energy of air flow into mechanical energy through rotation. According to [22], the maximum amount of mechanical power that can be generated by the turbine is as follows:

$$P_m = \frac{2}{3} \eta_{col} \eta_{ch} A_{col} \mathrm{G}. \tag{8}$$

The amount of electrical energy generated by the central solar chimney is determined by:

$$P_e = \frac{2}{3} \eta_{col} \eta_{turb} \frac{g}{C_p T_a} H_{ch} A_{col} \mathrm{G}. \tag{9}$$

4. INCORPORATION OF VEGETATION UNDER THE COLLECTOR ROOF OF SOLAR CHIMNEY POWER PLANTS

With vegetation added to the collector, the existing physical model (shown in Fig. 1) must be modified. As shown in Fig. 2, the collector is divided into two parts: one for vegetation and one for the ground. The vegetation is assumed to be planted all around the collector's circumference (360°), extending inward from the collector's perimeter to a determined radius (Rveg). This allows vegetation to be situated under the collector roof without suffering from the high temperatures near the chimney.

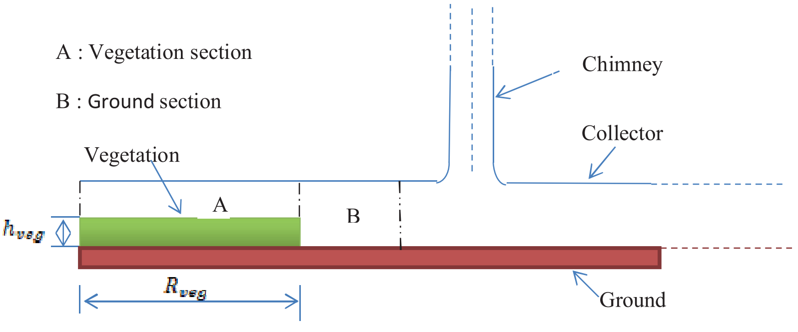

Fig. 2. The addition of vegetation under the collector roof creates two sections in the collector: the vegetation section and the ground section.

5. APPROACH FOR THE POROUS MEDIUM

Since the 1980s, the greenhouse climate uniformity assumption has been widely adopted for modelling heat and mass transfer. This assumption presumes that the greenhouse environment is perfectly uniform, with a single temperature and air speed assumed to be consistent near the walls and at ground level, or within the vegetation, which is typically modelled as a large, uniform-temperature "big leaf" [23].

Modelling the flow of heat, vapour, and momentum in a greenhouse is essential for understanding and predicting the crop's response to external physical factors. The complexity of defining and designing a 3D domain makes it challenging, but using vegetation as a porous medium is proposed as a solution [24], [25].

A porous material is composed of a solid matrix containing interconnected pores through which fluid can flow. The presence of the solid matrix significantly affects the transfer of properties such as momentum balance, as the friction on the matrix affects it. Darcy's law [26] is a simple model that explains the relationship between the pressure gradient and the velocity vector in a defined space.

$$gradP = -\frac{\mu}{K}u \, . \tag{10}$$

The intrinsic permeability of the porous medium, which only depends on its geometry, is represented by the coefficient K. This law does not include the inertia term and represents the momentum equation.

The validity of Darcy's law is defined by the modified Reynolds number [26].

$$\mathrm{Re}_P = \frac{U}{\nu}\sqrt{K}\,, \tag{11}$$

where U – wind speed and ν – the air's kinematic viscosity.

Many experiments have verified Darcy's law, but it only applies when the fluid flow is slow and the Reynolds number (Re_P) is below one based on typical pore size. This means that friction resistance is more significant than resistance due to changes in flow direction. Furthermore, there is a transition domain ($1 \prec \mathrm{Re}_P \prec 10$). When this occurs $\mathrm{Re}_P \succ 10$, the pressure gradient is influenced by both the flow speed and its square. This is true even if the flow within the pores does not turn turbulent, as the resistance to flow caused by friction is similar to the resistance due to the shape of the pores (which causes changes in flow direction). The Darcy equation (10) must then be revised by incorporating a factor that depends on the velocity squared; this results in the Darcy-Forchheimer equation [26].

$$gradP = -\frac{\mu}{K}u - \frac{c_F}{\sqrt{K}}\rho u U\,, \tag{12}$$

where ρ is the fluid's density and c_F is a dimensionless factor that depends on the characteristics of the porous medium, referred to as the inertial factor or nonlinear pressure drop coefficient. Initially considered c_F was a universal constant of the order of 0.55; however, it was later found to vary between 0.1 and 0.61, depending on the porous medium's composition [26].

In greenhouse conditions where the crop's permeability is substantial (the order of magnitude of dynamic viscosity μ is 10^{-5} for air), the pressure gradient is only influenced by the quadratic term as the viscous term is negligible [26].

$$gradP \approx -\frac{c_F}{\sqrt{K}}\rho u U\,, \tag{13}$$

where u – the velocity vector; U – the wind speed.

6. FLOW INTERACTION WITH VEGETATION COVER

The interaction between a plant canopy and air flow causes a decrease in momentum and increased absorption of solar energy by the leaves. This includes heat, water vapour release through transpiration, and exchanges in photosynthesis. These factors must be taken into account when using computational fluid dynamics (CFDs). The loss of momentum is due to the impact of the pressure gradient (*gradP*), as represented by a commonly used formula in [26].

$$gradP = L_l C_\nu \rho u U\,, \tag{14}$$

where L_l is the leaf area, u is the air velocity, and C_ν is the friction coefficient.

Studies [26], [27] combined this technology with a porous media approach. The inertial factor and permeability of the porous media are determined based on the plant's characteristics using the relationship.

$$\frac{C_F}{\sqrt{K}} = L_l C_\nu\,. \tag{15}$$

7. BOUNDARY CONDITIONS

Table 1 illustrates the physical model's boundary conditions. The roof of the collector is treated with a convection boundary condition, where the heat transfer coefficient from the collector roof to the environment is computed by Pretorius and Kröger [28]. The solar insolation that enters the computational domain through the semi-transparent collector cover is acquired from data sources [6], [29].

In a Solar Chimney Power Plant, a wind turbine that operates in stages of pressure is positioned at the base of the chimney. This design keeps the air velocity unchanged both before and after the turbine. To determine the pressure differential across the turbine during simulations, an iterative process was employed [9].

Table 1. Boundary Conditions

Place	Type	Value
Sides of the heat storage layer	Wall	Adiabatic
Bottom	Wall	T=330K
Cover of the collector	Wall (semi-transparent)	Mixed, h=9.5$W.m^{-2}.K^{-1}$, T_a = *Tambiante* solar irradiation
Surface of the chimney and junction	Wall	Adiabatic
Axe	Axis	Symmetry
Collector inlet	Pressure inlet	$P_{gage} = 0Pa$
Chimney outlet	Pressure outlet	$P_{gage} = 0Pa$
Pressure drop across the turbine	Reverse fan	Calculated by the iterative approach

8. BOUNDARY CONDITIONS AND PHYSICAL PROPERTIES OF THE SYSTEM

The main settings of the CFD simulation are outlined in Table 2a, and the construction materials and their physical properties are presented in Table 2b. Furthermore, a portion of the ground surface area is covered with vegetation under the collector roof (as seen in Fig. 2) with dimensions specified in Table 3.

Table 2a. Boundary Conditions

Classification	Setting	Classification	Setting
Solver	-Pressure-based coupled algorithm. -2D axisymmetric simulation. -Steady state (second-order upwind discretization).	Viscous model	- RNG $k-\varepsilon$ model. - Full buoyancy effects.
Energy equation	-Activated.	Radiation model	- DO (discrete ordinates). - Theta divisions: 3. - Phi divisions: 5. - Theta pixels: 3. - Phi pixels: 5.

Table 2b. Physical Properties of Materials [28]

Physical property (unit)	Glass (collector roof)		Ground (soil)	Chimney (concrete)
Wavelength band	Visible (0.1 – 3) μm	Infrared (3 – 100) μm	-	-
Absorption coefficient	0.04	0.95	0.90	0.60
Transmission coefficient	0.92	0.05	0	0
Absorption coefficient (m^{-1})	30	104	-	-
Emissivity	0.9		0.9	0.71
Refractive index	1.526		-	-
Extinction coefficient (m^{-1})	4		-	-
Density (kg/m^3)	2700		2160	2100
Specific heat (*J/Kg.K*)	840		710	880
Thermal Conductivity (*W/m.K*)	0.78		1.83	1.40
Thickness (*m*)	0.004		-	-
Surface roughness (*m*)	0		0.05	0.002

Table 3. Physical Properties of Vegetation [30]–[34]

Physical properties of vegetation	
Density (kg/m^3)	800
Specific heat capacity (*J/Kg.K*)	3224.7
Thermal conductivity (*W/m.K*)	0.213
Emissivity	0.98
Absorptivity	0.77
Surface roughness (*m*)	0.1
The height of vegetation hveg (*m*)	0.3
Radial distance from perimeter (*m*)	106.5

9. PARAMETERS EMPLOYED IN THE POROUS MEDIA MODEL

The vegetation cover is modelled as a porous medium using the Fluent 17.1 program for solving fluid dynamics equations, which combines the traditional porous medium approach with the discretization of Darcy and Forchheimer equations. The vegetation cover in this study consists of a row of young cowpea plants surrounding the collector in a 360° orientation, extending to a specified radius, Rveg, with a height of 0.3 m. The intrinsic permeability of the porous medium is defined as K = 0.884 and the non-linear pressure drop coefficient as = 1 [26].

10. SIMULATION AND RESULTS

Four numerical simulations are conducted: (1) solar chimney power plant without radiation and vegetation, (2) solar chimney power plant with radiation and no vegetation, (3) solar chimney power plant without radiation but with vegetation, and

(4) solar chimney power plant with radiation and vegetation. These simulations are based on the previously described plant specifications, the properties of the vegetation, and an assumed maximum temperature of 39 °C at which the vegetation can operate without disrupting photosynthesis (lower than the values determined in [34]). The study examines the inclusion of vegetation under the collector roof, extending from the collector perimeter to radii of Rveg = 106.5m.

The temperature and velocity profiles of the fluid in the collector with and without vegetation are shown in Figs. 3 and 4, respectively, for a specific solar radiation level ($Q = 1000\ W/m^2$). The temperature and velocity of the fluid increase as the radius decreases and approaches the base of the chimney. Figure 3 displays the air velocity profiles through the collector, and it can be seen that in the vegetation zone, the speed decreases slightly before gradually increasing closer to the base of the chimney. The highest temperature and velocity of the fluid are recorded in the solar chimney power plant without vegetation and with radiation, as seen in Figs. 3 and 4. This indicates that both the presence of vegetation and radiation play a role in the performance of the solar chimney power plant.

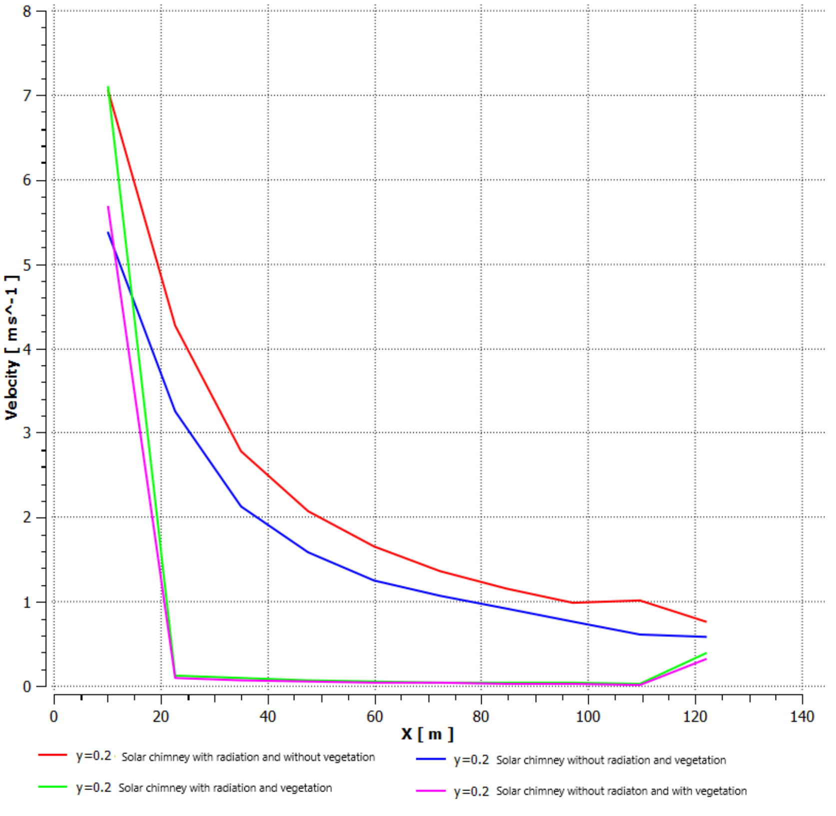

Fig. 3. Velocity profile of the different SCPP systems in the collector at (R_{veg} = 106.5 m), Y = 0.2 and $T_{sol\text{-}air}$ = 324K and solar insolation of 1000 W / m².

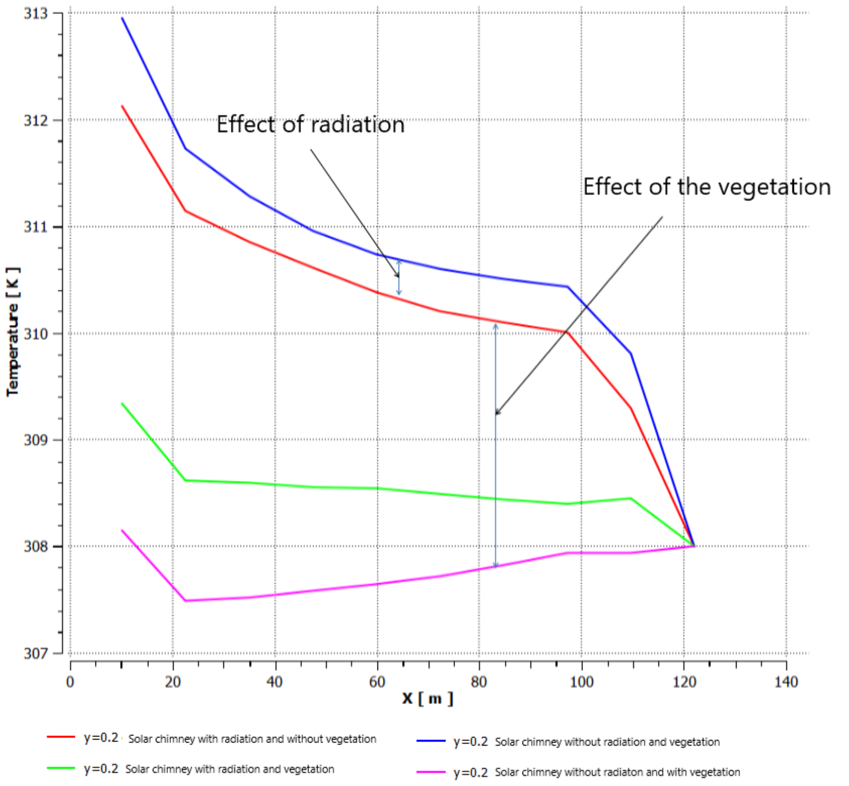

Fig. 4. Temperature profile of the different SCPP systems in the collector at (R_{veg} = 106.5 m), Y = 0.2 and $T_{sol\text{-}air}$ = 324K and solar insolation of 1000 W / m^2.

The simulations of the reference plant, secondary collector roof, and secondary and tertiary collector roof systems have been carried out as outlined in [11]. The results, shown in Table 4, demonstrate that the secondary and tertiary collector roof systems generate the most electricity compared to the other systems. However, incorporating vegetation into a solar chimney power plant reduces the electricity production as compared to solar chimney systems without vegetation. Adding vegetation may be a possibility, but it leads to a significant decrease in the power output of the plant.

Table 4. The Comparison of Power Output at a Solar Irradiation of 1000 W/m2 and a Ground Temperature of 324 K

Systems	Power output (Kw)	
	With vegetation	Without vegetation
Reference plant	31.2	50.01
Plant with secondary collector roof	39.6	59.7
Plant with secondary and tertiary collector roof	60.04	80.2

The functioning of solar systems is strongly tied to the amount of solar radiation received. Our initial focus was on this key factor. The German Special Agency states that Algeria has a higher solar potential compared to other countries in the Mediterranean region [35].

This study focuses on Tamanrasset, a city in southern Algeria with an ideal location for utilising solar energy and its associated technologies. The city's geographical coordinates are listed in Table 5. We obtained the average monthly daily solar radiation data, measured in MJ/m2/day, from various national and international databases, including the Solar Atlas of Algeria [29], [6], the Photovoltaic Geographical Information System, and Metronome, which is a commercial data source.

The Tamanrasset region is in the southern part of Algeria and boasts a dry Saharan climate with abundant sunshine and flat, unused areas, making it an ideal location for solar energy utilisation and the adoption of SCPP technology. This will provide electric power to remote villages in southern Algeria. Additionally, harnessing thermal energy in the collector zone through greenhouse farming practices will significantly reduce the cost of energy production.

Table 5. Geographical Coordinates of Tamanrasset Region

Sites	Lat. °N	Long. °E	Alt. (m)	Climate
Tamanrasset	22.8	5.5	1381	Arid

Figure 5 displays the monthly variations in solar radiation in the Tamanrasset region. It can be seen that Tamanrasset experiences high levels of solar radiation (28.8 MJ/m2/day), and the highest levels occur in June.

Figure 6 illustrates the variations in the average ambient temperature of the Tamanrasset region throughout the year. The average ambient temperature in Tamanrasset can reach 29 °C.

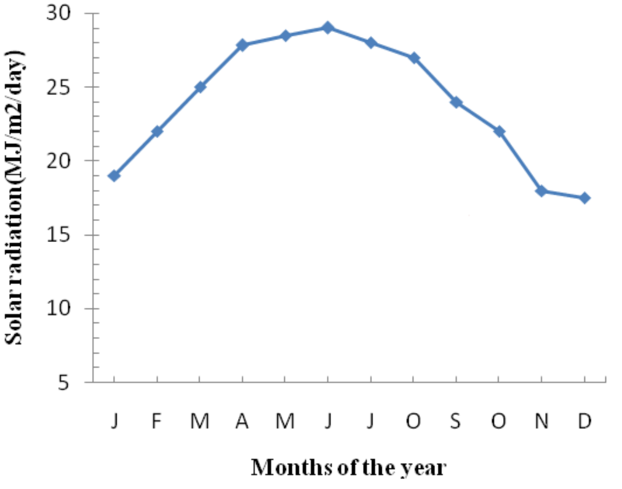

Fig. 5. Monthly solar radiation in the Tamanrasset region.

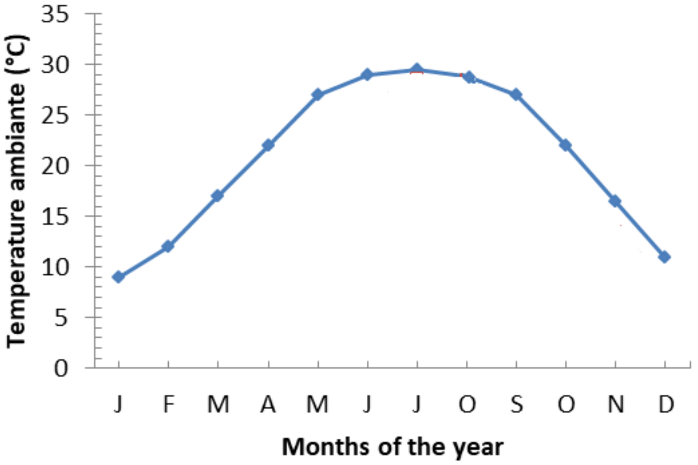

Fig. 6. Monthly ambient temperature in the Tamanrasset region.

Three numerical simulations were conducted based on the plant specifications, vegetation properties, and maximum temperature for vegetation survival, as described in [11]. The simulations involved the reference plant, a secondary collector roof, and systems with secondary and tertiary collector roofs. This section covers the integration of vegetation under the collector roof, from the collector's edge to the Rveg rays of the collector.

By comparing the three systems at Tamanrasset, the reference plant, secondary collector roof, and secondary and tertiary collector roof systems (detailed in [11]), we found that the secondary and tertiary collector roof systems generated the most electricity, as shown in Figs. 7– 9. They display the monthly electricity generated by SCPP located in the Tamanrasset region. The figures indicate that the reference solar chimney with vegetation (without a secondary collector roof) produces less electricity than the reference solar chimney without vegetation.

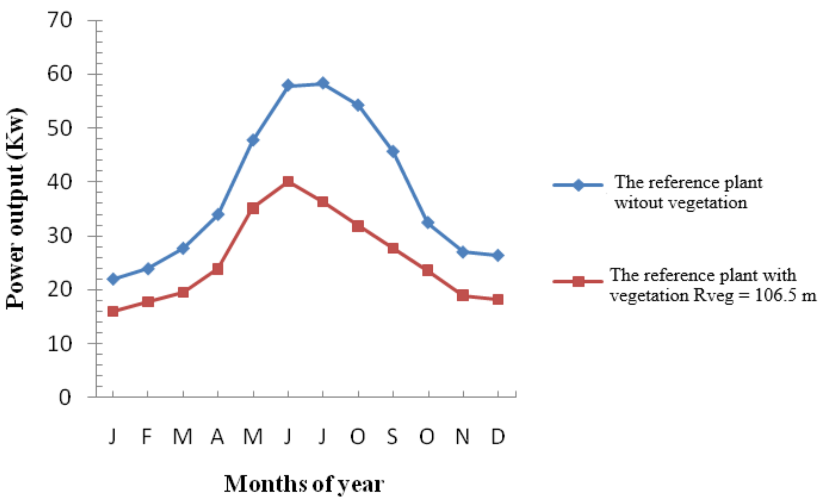

Fig. 7. Monthly average productivity of the power of the solar chimney at Tamanrasset.

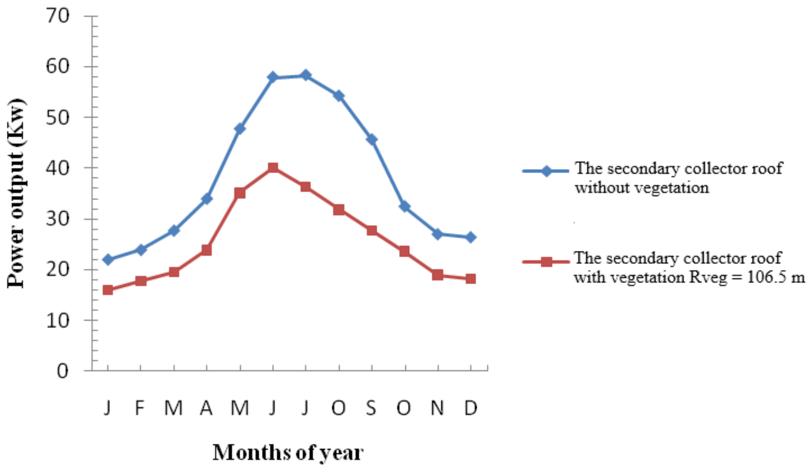

Fig. 8. Monthly average productivity of the power of the solar chimney at Tamanrasset.

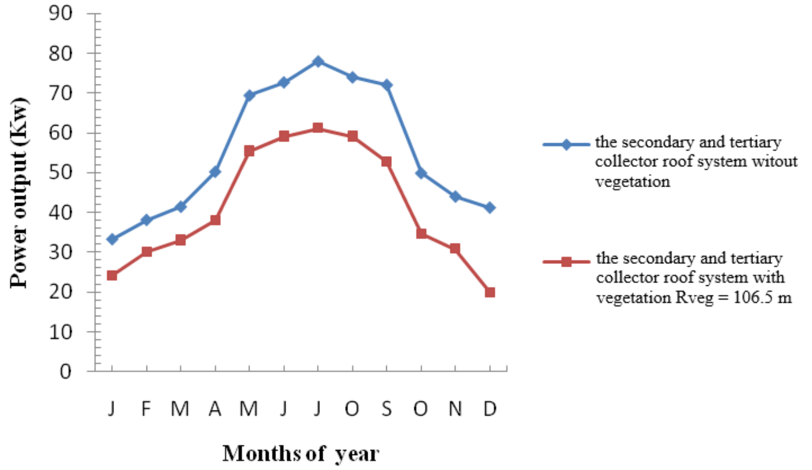

Fig. 9. Monthly average productivity of the power of the solar chimney at Tamanrasset.

12. CONCLUSIONS

This paper presents a numerical study of solar chimney power plants with and without the presence of vegetation. The main aim is to evaluate the impact of vegetation on the plant's power output when placed under the collector roof. We analysed the performance of different solar chimney power plant configurations with and without vegetation under the collectors.

We included the reference plant, a secondary collector roof, and systems with secondary and tertiary collector roofs. According to the findings, the secondary and tertiary collector roof system had the greatest electricity production, generating an annual output of 34 to 80 kW. The results indicate that incorporating vegetation into a solar chimney power plant may be possible, but it will result in significant reductions in the plant's power output.

ACKNOWLEDGEMENTS

This research has been supported by the Ministry of Higher Education and Scientific Research, Algeria (Grant Reference Number A10N01UN110120230001). We are very grateful to our Research Laboratory for their great help in making part of this work to be done.

REFERENCES

1. Dhahri, A., & Omri, A. (2013). A Review of Solar Chimney Power Generation Technology. *International Journal of Engineering and Advanced Technology, 2* (3), 1–17.
2. Heisler, E. M. (2014). *Exploring Alternative Designs for Solar Chimneys Using Computational Fluid Dynamics*. Thesis.
3. Humphries, M. (2001). *Solar Tower in Arizona to Power 150,000 Homes for 80 years*. GEEK. [Online]. Available: http://www.geek.com/geek-pick/solar-tower-in-arizona-to-power-150000-homes-for-80-years-1406459/
4. Tahar, T., & Djezzar, M. (2021). Numerical Simulation of Natural Convection in a Solar Chimney. *International Journal of Renewable Energy Research, 2* (4), 712–717.
5. Haaf, W., Friedrich, K., Mayer, G., & Schlaich, J. (1983). Solar Chimneys. *Int J Sol Energy*, *2*, 3–20.
6. Rabehi, R., Chaker, A., Aouachria, Z., & Tingzhen, M. (2017). CFD Analysis on the Performance of a Solar Chimney Power Plant System: Case Studying Algeria. *International Journal of Green Energy*, *14* (12), 971–982.
7. Hu, S., Leung, D. Y., Chen, M. Z., & Chan, J. C. (2016). Effect of Guide Wall on the Potential of a Solar Chimney Power Plant. *Renewable Energy, 96*, 209–219.
8. Hafizh, H. (2015). *Theoretical Analysis and Experimental Optimization of Solar Updraft Power Generator.* PhD Thesis.
9. Gholamalizadeh, E., & Kim, M.-H. (2014). Three-Dimensional CFD Analysis for Simulating the Greenhouse Effect in Solar Chimney Power Plants Using a Two-Band Radiation Model. *Renewable Energy*, *63*, 498–506.
10. Cao, F., Li, H., Zhao, L., Bao, T., & Guo, L. (2013). Design and Simulation of the Solar Chimney Power Plants with TRNSYS. *Solar Energy, 98,* 23–33.
11. Djaouida, B., Aouachria, Z., Benmachiche, A. H., & Ali, S. (2020). Controlling Power Output of Solar Chimney Power Plant according to Demand. *International Journal of Ambient Energy, 41* (13), 1467–1481.
12. Ali, S., Djaouida, B., Benmachiche, A. H., & Aouachria, Z. (2021). Performance Analysis of a Solar Chimney Power Plant System in Two Algeria Regions. *International Journal of Ambient Energy, 43* (6), 1–26.
13. Ming, T., Wang, X., De Richter, R. K., Liu, W., Wu, T., & Pan, Y. (2012). Numerical Analysis on the Influence of Ambient Crosswind on the Performance of Solar Updraft Power Plant System. *Renewable and Sustainable Energy Reviews, 16* (8), 5567–5583.
14. Huang, H., Zhang, H., Huang, Y., & Lu, F. (2007). Simulation Calculation on Solar Chimney Power Plant System. *Challenges of Power Engineering and Environment*: Springer, 1158–1161.
15. Guo, P., Li, J., Wang, Y., & Wang, Y. (2015). Numerical Study on the Performance of a Solar Chimney Power Plant. *Energy Conversion and Management, 105,* 197–205.

16. Nasirivatan, S., Kasaeian, A., Ghalamchi, M., & Ghalamchi, M. (2015). Performance Optimization of Solar Chimney Power Plant Using Electric/Corona Wind. *Journal of Electrostatics, 78,* 22–30.
17. Ghalamchi, M., Kasaeian, A., Ghalamchi, M., & Mirzahosseini, A. H. (2016). An Experimental Study on the Thermal Performance of a Solar Chimney with Different Dimensional Parameters. *Renewable Energy, 91,* 477–483.
18. Liu, S., & Li, Y. (2015). Heating Performance of a Solar Chimney Combined PCM: A Numerical Case Study. *Energy and Buildings, 99*, 117–130.
19. Li, Y., & Liu, S. (2014). Numerical Study on Thermal Behaviors of a Solar Chimney Incorporated with PCM. *Energy and Buildings, 80*, 406–414.
20. Attig, B.F., Guellouz, M.S., Sahraoui, M., & Kaddeche, S. (2015). A Numerical Study of Solar Chimney Power Plants in Tunisia. *Journal of Physics: Conference Series, 596* (1), 012006.
21. Akhtar, Z., & Rao, K.V.S. (2014). Study of economic viability of 200 MW solar chimney power plant in Rajasthan, India. *1st International Conference on Non-conventional Energy (ICONCE 2014),* (pp. 84–88). Kalyani, India.
22. Schlaich, J. (1995). *The Solar Chimney: Electricity from the Sun*. Germany: Geislingen.
23. Ould Khaoua, S.A. (2006). *Modélisation de l'aération naturelle et du microclimat des serres en verre de grande portée sous climat tempéré océanique.* Thèse de Doctorat, Ecole Doctorale d'Angers.
24. Boulard, T., Kittas, C., Roy, J. C., & Wang, S. (2002). Convective and Ventilation Transfers in Greenhouses, Part 2: Determination of the Distributed Greenhouse Climate. *Biosystèms Engineering, 83* (2), 129–147.
25. Majdoubi, H., Boulard, T., Fatnassi, H., & Bouirden, L. (2009). Airflow and Microclimate Patterns in a One-Hectare Canary Type Greenhouse: An Experimental and CFD Assisted Study. *Agricultural and Forest Meteorology, 149,* 6–7.
26. Haxaire, R. (1999). *Caractérisation et modélisation des écoulements d'air dans une serre*. Thèse de Doctorat, Université de Nice Sophia Antipolis.
27. Boulard, T., & Wang, S. (2002). Experimental and Numerical Studies on the Heterogeneity of Crop Transpiration in a Plastic Tunnel. *Computers and Electronics in Agriculture, 34*, 173–190.
28. Pretorius, J. P., & Kröger, D. G. (2006). Solar Chimney Power Plant Performance. *J Sol Energy Eng., 128,* 302–311.
29. Yaiche, M. R., Bouhanik, A., Bekkouche, S.M.A., Malek, A., & Benouaz, T. (2014). Revised Solar Maps of Algeria Based on Sunshine Duration. *Energy Conversion and Management, 82,* 114–23.
30. Mahapatra, A. K., Melton, S. L., & Isang, E. M. (2013). Effect of Moisture Content on Thermal Properties of Cowpea Flours. *Agric Eng Int: CIGR Journal, 15* (2).
31. Arku, A.Y., Aviara, N.A., & Ahamefula, S.C. (2012). Specific Heat of Selected Legumes and Cereal Grains Grown in North Eastern Nigeria. *Arid Zone Journal of Engineering, Technology and Environment, 8*, 105–114.
32. Appiah, F., Asibuo, J. Y., & Kumah, P. (2011). Physicochemical and Functional Properties of Bean Flours of Three Cowpea (Vigna unguiculata L. Walp) Varieties in Ghana. *African Journal of Food Science, 5* (2), 100–104.
33. Pretorius, J. P., & Kroger, D. G. (2008). Incorporating Vegetation under the Collector Roof of a Solar Chimney Power Plant. *R & D Journal, 24* (l), 3–11.
34. Wahid, A., Gelani, S., Ashraf, M., & Foolad, M. R. (2007). Heat Tolerance in Plants: An Overview. *Environmental and Experimental Botany, 61,* 199–223.
35. Mefti, A., Bouroubi, M. Y., & Mimouni, H. (2002). Evaluation du potentiel énergétique solaire. *Bulletin des Energies Renouvelables, 2*.